ACSNANO

www.acsnano.org

ARTICLE

Ligand-Mediated Synthesis of Shape-Controlled Cesium Lead Halide Perovskite Nanocrystals *via* Reprecipitation Process at Room Temperature

Shibin Sun, Dan Yuan, Yuan Xu, Aifei Wang, and Zhengtao Deng*

Department of Biomedical Engineering, College of Engineering and Applied Sciences, Nanjing National Laboratory of Microstructures, Collaborative Innovation Center of Advanced Microstructures, Nanjing University, Nanjing, Jiangsu 210093, P. R. China

Supporting Information

ABSTRACT: **Colloidal nanocrystals of fully inorganic cesium lead halide ($CsPbX_3$, X = Cl, Br, I, or combinations thereof) perovskites have attracted much attention for photonic and optoelectronic applications. Herein, we demonstrate a facile room-temperature (*e.g.*, 25 °C), ligand-mediated reprecipitation strategy for systematically manipulating the shape of $CsPbX_3$ colloidal nanocrystals, such as spherical quantum dots, nanocubes, nanorods, and nanoplatelets. The colloidal spherical quantum dots of $CsPbX_3$ were synthesized with photoluminescence (PL) quantum yield values up to >80%, and the corresponding PL emission peaks covering the visible range from 380 to 693 nm. Besides spherical quantum dots, the shape of $CsPbX_3$ nanocrystals could be engineered into nanocubes, one-dimensional nanorods, and two-dimensional few-unit-cell-thick nanoplatelets with well-defined morphology by choosing different organic acid and amine ligands *via* the reprecipitation process. The shape-dependent PL decay lifetimes have been determined to be several to tens to hundreds of nanoseconds. Our method provides a facile and versatile route to rationally control the shape of the $CsPbX_3$ perovskites nanocrystals, which will create opportunities for applications such as displays, lasing, light-emitting diodes, solar concentrators, and photon detection.**

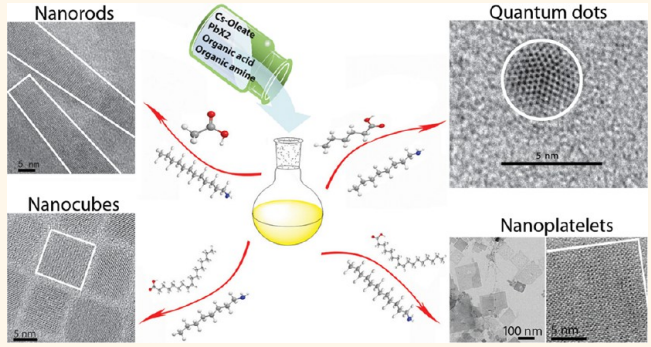

KEYWORDS: *perovskite, cesium lead halide, nanocrystals, quantum dots, nanocubes, nanorods, nanoplatelets*

The past few years have witnessed important progress demonstrating outstanding optoelectronic characteristics of organic−inorganic lead−halide-based perovskites in the form of thin films, microcrystals and bulk single crystals, which are emerging as one of the most promising materials for solution-processable photovoltaic technology.[1−3] Recent reports on inexpensive photovoltaic devices with certified power conversion efficiencies over 20% using hybrid organic−inorganic lead halides $MAPbX_3$ ($MA = CH_3NH_3^+$, $X = Cl^-$, Br^-, and I^-) as semiconducting absorber layers are highly encouraging.[4−6] In addition, researchers recently reported the synthesis of nanoscale crystallite of organic−inorganic lead halides $MAPbX_3$, such as zero-dimensional (0D) spherical quantum dots, one-dimensional (1D) nanowires, and two-dimensional (2D) nanoplatelets.[7−9] In particular, single-crystalline 2D hybrid perovskites of $(C_4H_9NH_3)_2PbBr_4$ nanoplatelets have recently been synthesized using a solution-phase growth method.[10]

With similarly high optoelectronic quality, such as small exciton binding energy, high thermal stability, and balanced electron and hole mobility lifetime, all-inorganic perovskites like AMX_3 (typically $A = Rb^+$, Cs^+; $M = Ge^{2+}$, Sn^{2+}, Pb^{2+}; $X = F^-$, Cl^-, Br^-, I^-, or combinations thereof) have great potential in applications, including high-efficiency photovoltaic cells, light-emitting-diodes, lasers, and photodetectors.[2,11−13] Research into $CsPbX_3$ has existed for more than a century.[14] The synthesis, crystallography, and photoconductivity of direct bandgap $CsPbX_3$ have been reported half a century ago.[15,16] However, there are limited reports for the synthesis of colloidal

Received: December 28, 2015
Accepted: February 17, 2016
Published: February 17, 2016

DOI: 10.1021/acsnano.5b08193
ACS Nano 2016, 10, 3648−3657

$CsPbX_3$ nanocrystals.[11,17,18] Until 2015, colloidal $CsPbX_3$ perovskites nanocubes and nanowires have been reported using a high-temperature (*e.g.*, 150−250 °C), hot-injection approach.[11,17] In particular, the reported $CsPbX_3$ nanocubes have size-tunable emissions from 410 to 700 nm, characterized by narrow emission line widths of 12−42 nm and high quantum yields reaching 90%. Moreover, $CsPbX_3$ nanocubes appear to be largely free from mid-gap trap states, which enable their advantages over the Cd−chalcogenide working in the blue-green spectral region of 410−530 nm.[17,19] It is worth to note that the photoluminescence (PL) emission spectra of these $CsPbX_3$ nanocrystals could be tunable over the entire visible spectral region by anion exchange reactions.[20,21] These progresses suggest $CsPbX_3$ nanocrystals hold great potential for both fundamental researches and industrial applications.[12,22,23]

The ability to systematically manipulate the shape or the morphology of inorganic nanocrystals remains an important goal of modern nanochemistry.[24] The geometric shape and size of inorganic nanocrystals control their physical properties, and changes in shape can modulate overall optical and electronic properties due to changes in band structure.[25] For example, the PL from spherical quantum dots is isotropic, whereas nanorods exhibit polarized emission.[25] To date, the best-developed nanocrystals in terms of size, shape, and composition are binary, ternary, and quaternary metal chalcogenide nanocrystals.[24,25] In contrast, the shape-controlled synthesis of all-inorganic AMX_3 perovskites nanocrystals remains rather unexplored.[9,11,26] It is, therefore, essential to determine the shape of $CsPbX_3$ nanocrystals so as to link morphology with performance in optical and optoelectronic applications.

Here, we report a facile ligand-assisted, room-temperature reprecipitation strategy for colloidal synthesis of zero-dimensional (0D) spherical quantum dots, nanocubes, one-dimensional (1D) nanorods, and two-dimensional (2D) few-unit-cell-thick nanoplatelets of $CsPbX_3$ nanocrystals with well-defined morphology (see Figure 1 and Table S1 in the Supporting Information). Although very recent reports[27,28] have noted the synthesis of $CsPbX_3$ nanocrystals at room temperature, the systematic investigation of their shape controlled synthesis is still lacking. We demonstrated that hexanoic acid and octylamine could tailor the nanocrystals into spherical quantum dots; oleic acid and dodecylamine would shape the nanocrystals into nanocubes; acetate acid and dodecylamine would shape the nanocrystals into nanocubes, while the oleic acid and octylamine would transform the nanocrystals into nanoplatelets. $CsPbX_3$ nanocrystals exhibit shape-dependent PL decay lifetime variable from several to tens to hundreds of nanoseconds and PL emission spectra tunable over the whole visible spectral region.

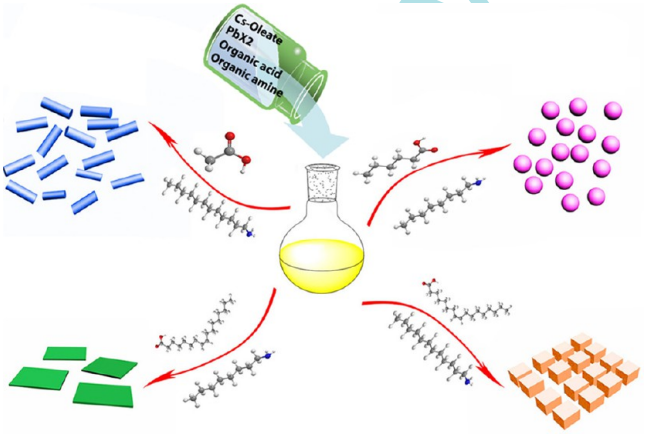

Figure 1. Schematic illustrating the formation process for different $CsPbX_3$ (X = Cl, Br, I) nanocrystals mediated by organic acid and amine ligands at room temperature. Hexanoic acid and octylamine for spherical quantum dots; oleic acid and dodecylamine for nanocubes; acetate acid and dodecylamine for nanorods; oleic acid and octylamine for few-unit-cell-thick nanoplatelets.

RESULTS AND DISCUSSION

The reprecipitation strategy for synthesis of $CsPbX_3$ ($X = Cl^-$, Br^-, I^-) spherical quantum dots was performed by mixing a solution of precursors in good solvent (such as *N*,*N*-dimethylformamide, DMF; tetrahydrofuran, THF; and dimethyl sulfoxide, DMSO) into a poor solvent (such as toluene and hexane) at room temperature, *i.e.*, 25 °C. Previously, reprecipitation process was used for preparation of polymers and $CH_3NH_3PbBr_3$ quantum dots.[7,27,29,30] The details for the synthesis can be found in Materials and Methods. As the reaction proceeded, the solution gradually changed its color, implying the formation of $CsPbX_3$ due to the co-precipitation of Cs^+, Pb^{2+}, and X^- in the presence of the organic acid and amine ligands. In the precursor solution, polar solvent (*e.g.*, DMF) acts as a good solvent to dissolve the inorganic salts and molecule ligands, while the nonpolar solvent (*e.g.*, toluene) acts as a bad solvent to promote the reprecipitation process.

Figures 2A−D and S1 show the typical transmission electron microscopy (TEM) and high-resolution transmission electron microscopy (HRTEM) images of spherical $CsPbBr_3$ quantum dots as well as the size distribution; it is observed that typical $CsPbBr_3$ quantum dots have an average diameter of 4.3 nm with a size deviation of ±0.8 nm (Figure 2F). From the HRTEM images (Figure 2C,D), interplanar distances of 3.4 Å corresponding to the (111) crystal plane can be easily identified, which is consistent with the Inorganic Crystal Structure Database (ICSD) Collection Code #97851, or the JCPDF #01-072-7929. As shown in Figure 2E, our strategy could be easily scaled up to produce 0.5 L of highly fluorescent small-sized $CsPbBr_3$ colloidal solution. It is worthy to note that the fluorescence of the colloidal solution could be directly seen under normal room light without using additional excitation light source. To analyze the phase structure, X-ray diffraction (XRD) patterns determinations were applied to characterize the obtained samples. Figure 2G shows XRD pattern of the product, where the peaks at 2θ = 15.1, 21.5, 30.4, 34.2, and 37.6° correspond to diffractions from {001}, {110}, {002}, {210}, and {211} planes of orthorhombic $CsPbBr_3$. The XRD data confirmed the formation of $CsPbBr_3$ quantum dots with space group *Pbnm*(62), which is consistent with the JCPDF #01-072-7929. No other phases were detected.

To analyze the optical properties, the colloidal solution of $CsPbBr_3$ quantum dots was examined by UV−vis absorption and PL emission and excitation spectra (Figure 2H). The absorption onset of $CsPbBr_3$ quantum dots is around 500 nm. The PL emission spectrum shows a peak position at 505 nm (2.46 eV) with excitation at 385 nm. The excitation spectrum shows that $CsPbBr_3$ quantum dots sample exhibit the strongest peak at 485 nm monitored at the emission wavelength of 505 nm, which is in good agreement with the result from the UV−vis absorption spectrum. Because of the smaller size of $CsPbBr_3$ quantum dots (~4.3 nm) relative to its exciton Bohr radius (~7.0 nm),[21] the observed blue shift of $CsPbBr_3$ quantum dots

DOI: 10.1021/acsnano.5b08193
ACS Nano 2016, 10, 3648−3657

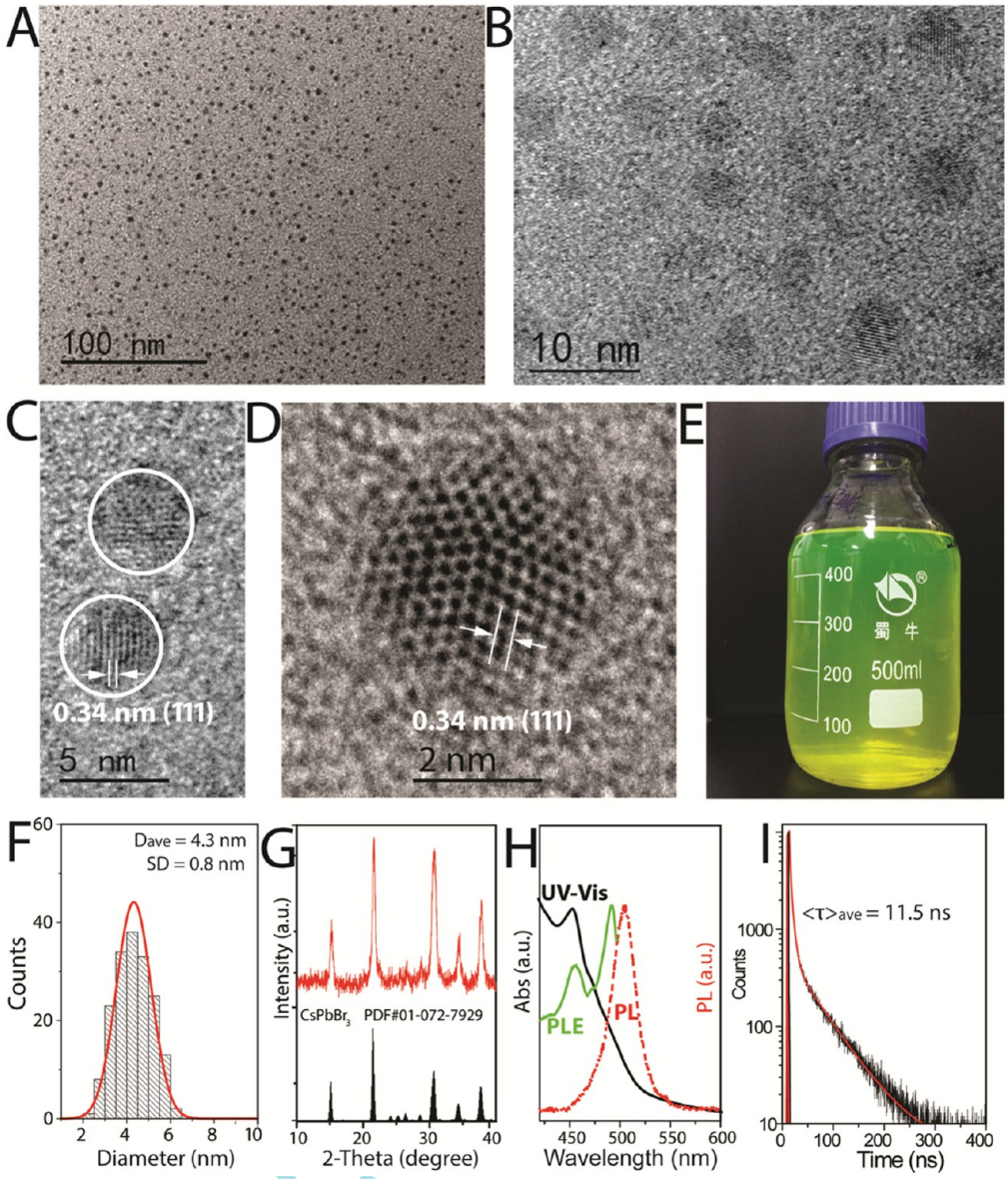

Figure 2. $CsPbBr_3$ spherical quantum dots synthesized using hexanoic acid and octylamine as ligands at room temperature, *i.e.*, 25 °C. (A–D) Low- and high-resolution TEM images of $CsPbBr_3$ quantum dots. (E) Photographs of 0.5 L $CsPbBr_3$ spherical quantum dots colloidal solution under room light. It was taken under normal room light without using additional excitation light source, and the yellow-green color is from the fluorescence of $CsPbBr_3$ quantum dots. (F) Analysis of size distribution for the sample shown in panel A. (G) XRD pattern of the $CsPbBr_3$ spherical quantum dots. (H) Optical absorption (black line), PL emission (PL, red dash line), and PL excitation (PLE, green line)) spectra of the spherical $CsPbBr_3$ quantum dots. (I) Time-resolved PL decay and fitting curves of the light emission at 505 nm from $CsPbBr_3$ nanoplatelets with the excitation wavelength of 375 nm.

could be explained by the quantum confinement effect. The PL quantum yield was estimated to be ~0.81, by comparison with a standard sample (Rhodamine 101, QY = 100% in ethanol + 0.01 HCl) following a procedure reported in the literature.[31] The time-resolved PL decay spectra of the quantum dots are shown in Figure 2I. The time-resolved PL decay curve was of $CsPbBr_3$, quantum dots were fitted to triexponential decay functions, and average PL decay lifetimes of 11.5 ns were derived, which is compared to nanocubes (average lifetime of 1–22 ns) and thin films (average lifetime of ~3.9 ns), but smaller than bulk crystal (average PL lifetime of ~2500 ns).[12,32]

The emission peaks of as-prepared spherical quantum dots can be tuned in the region of 457, 465, 474, 510, and 515 nm by changing the temperature between −20, 0, 20, 40, and 60 °C of the bad solvent during reprecipitation, respectively. The TEM images shown in Figure S2 indicate the obtained samples at 40 °C are also in spherical dot shape with average diameter of 4.5 nm with a size deviation of ±0.9 nm. Optical absorption and emission spectra of selected spherical quantum dots (Figure 3A) show narrow emission line widths of 20–30 nm, indicating the narrow size distributions. The absorption and PL excitation spectra of the quantum dots also show a band edge red shift with increasing synthesis temperature. The quantum dot samples have a small 10–20 nm Stokes shift between the absorption edge and the emission peak (Figure 3A), which are consistent with a direct exciton recombination process. As shown in Figure S3, the experimental diameter values measured from TEM images can be fitted into a linear function of the PL

DOI: 10.1021/acsnano.5b08193
ACS Nano 2016, 10, 3648–3657

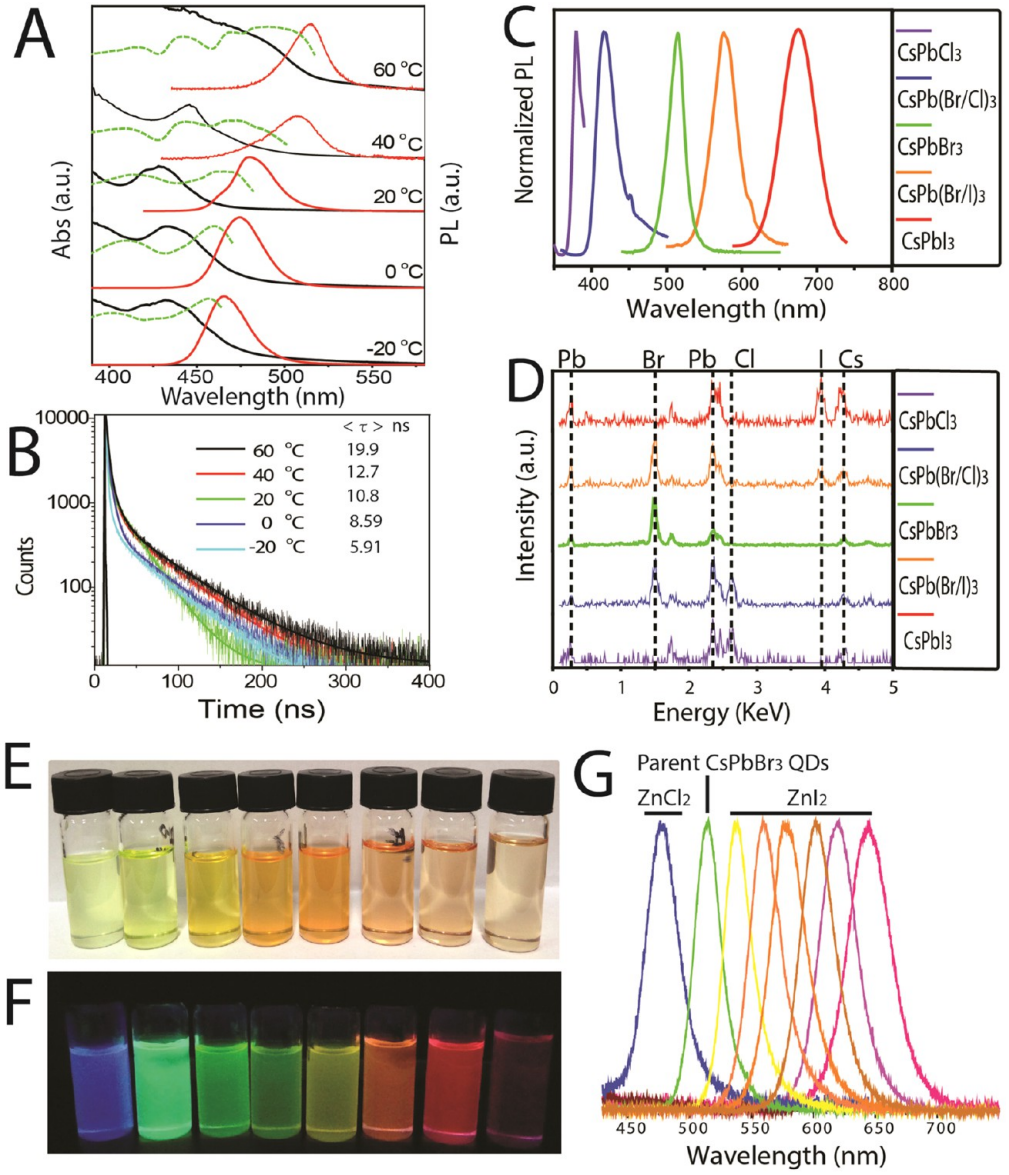

Figure 3. (A) Optical absorption (black line), PL excitation (green dash line), and PL emission (red line) spectra of different sized spherical $CsPbBr_3$ quantum dots synthesized at −20, 0, 20, 40, and 60 °C with PL emission peak at 457, 465, 474, 510, and 515 nm, respectively. (B) Time-resolved PL decay and fitting curves of different sized spherical $CsPbBr_3$ quantum dots synthesized at −20, 0, 20, 40, and 60 °C with average PL decay lifetime at 5.91, 8.59, 10.8, 12.7, and 19.9 ns, respectively. (C and D) PL emission and energy-dispersive spectroscopy (EDS) spectra of a series of $CsPbX_3$ (purple line, $CsPbCl_3$; blue line, $CsPbCl_{1.5}Br_{1.5}$; green line, $CsPbBr_3$; orange line, $CsPbCl_{1.5}Br_{1.5}$; red line, $CsPbI_3$) quantum dots with emission peaks at 380, 416, 515, 575, and 693 nm, respectively, synthesized at room temperature. (E and F) Anion exchange of the as-synthesized spherical $CsPbBr_3$ quantum dots with stable dispersions in toluene under room light or excitation using an ultraviolet lamp at room temperature. (G) PL spectra of the solutions shown in (E). The spectra of the parent $CsPbBr_3$ quantum dots and the resulting anion-exchanged $CsPbX_3$ quantum dots either by $ZnCl_2$ or ZnI_2 (with variable amount) salts are labeled. From left to right, the PL emission maxima (PL quantum yield) of the samples showing in panel E are 477 nm (49.3%), 514 nm (81.1%), 537 nm (56.5%), 560 nm (36.4%), 578 nm (20.6%), 603 nm (15.6%), 628 nm (11.3%), and 661 nm (6.8%), respectively.

emission peak position of the $CsPbBr_3$ quantum dots. Representative time-resolved PL decay spectra of the quantum dots synthesized at different temperature are shown in Figure 3B. The time-resolved PL decay curves were fitted to triexponential decay functions, and average PL decay lifetimes of 5.91, 8.59, 10.8, 12.7, and 19.9 ns were derived. The radiative lifetimes gradually increased as the emission shifts to longer wavelengths as the precipitation temperature is increased. The average PL decay lifetimes of colloidal $CsPbBr_3$ quantum dots were reduced with decreasing size. This suggests that the PL decay of colloidal $CsPbBr_3$ quantum dots mainly took place through exciton radiative recombination in the small nanocrystals.[19,32]

The synthesis of spherical $CsPbBr_3$ quantum dots is general for other $CsPbX_3$ quantum dots. For example, following a similar process by exchanging $PbBr_2$ with PbI_2, we synthesized $CsPbI_3$ spherical quantum dots with an average diameter of 5.0 nm with a size deviation of ±1.1 nm (see Figure S4). Figure 3D is an EDS spectrum obtained from the same spherical quantum dots. The Cs, Pb, and Cl, or Br, or I peaks are observed,

DOI: 10.1021/acsnano.5b08193
ACS Nano 2016, 10, 3648−3657

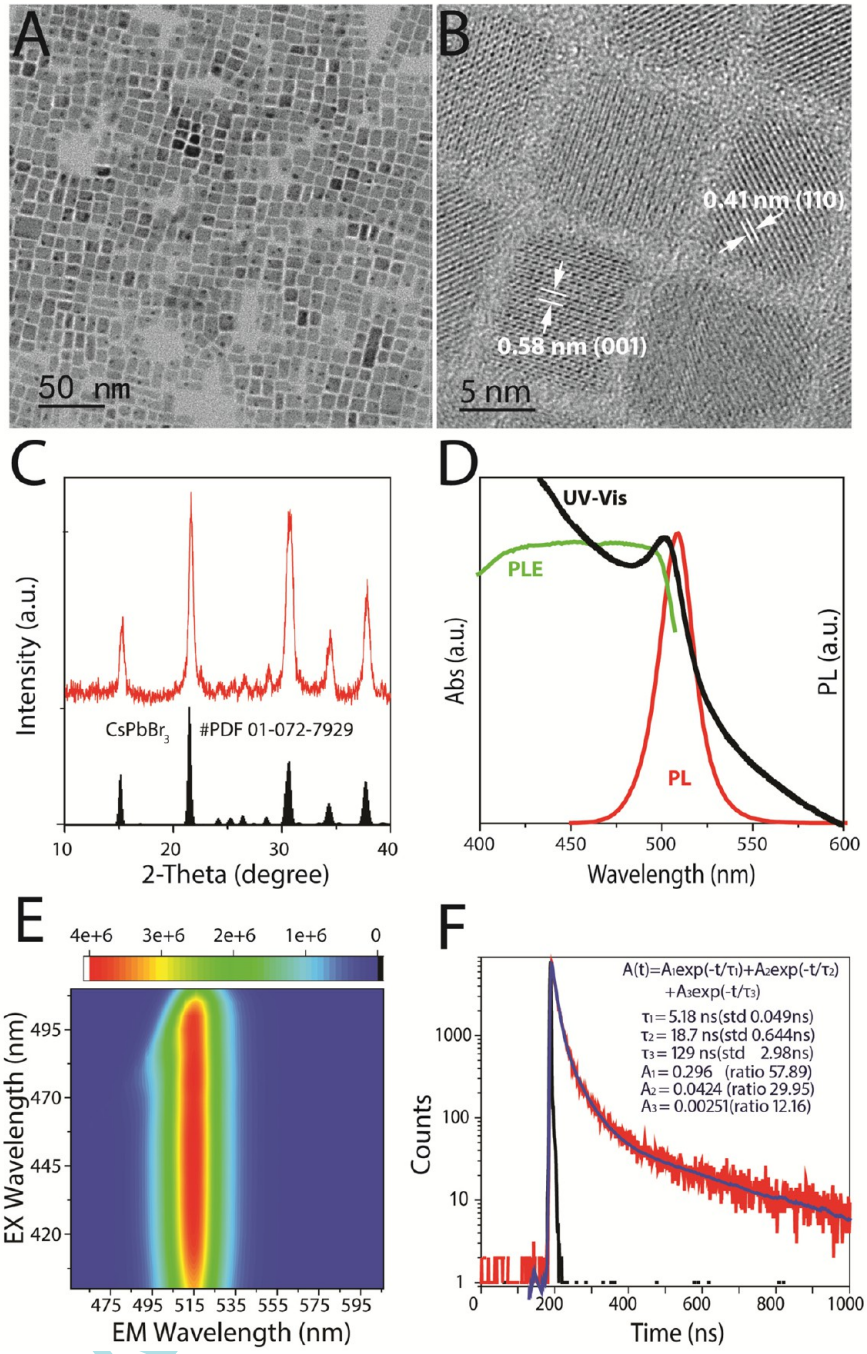

Figure 4. $CsPbBr_3$ nanocubes synthesized using oleic acid and dodecylamine as ligands at room temperature. (A) Low- and (B) high-resolution TEM images of $CsPbBr_3$ nanocubes. (C) XRD pattern of the $CsPbBr_3$ nanocubes. (D) Optical absorption (black line), PL excitation (green line), and PL emission (red line) spectra of the $CsPbBr_3$ nanocubes. (E) Graphical depictions of the pseudo colored PL intensity measured as a function of excitation wavelength. (F) Time-resolved PL decay and fitting curves of the light emission at 514 nm from $CsPbBr_3$ nanocubes with a 375 nm pulse laser.

suggesting that the quantum dots are composed of mainly Cs, Pb, and Cl, or Br, or I. The PL emission spectra (Figure 3C) and the EDS patterns (Figure 3D) reveal that the end product contains a large quantity of $CsPbCl_3$, $CsPbCl_{1.5}Br_{1.5}$, $CsPbBr_3$, $CsPbCl_{1.5}Br_{1.5}$, and $CsPbI_3$ spherical quantum dots with emission peaks at 380, 416, 515, 575, and 693 nm, respectively.

X-ray photoelectron spectroscopy (XPS) determinations were performed to further investigate the elemental composition of the as-synthesized colloidal $CsPbBr_3$ quantum dots. Figure S5 shows the survey X-ray photoelectron spectrum and high-resolution X-ray photoelectron spectra of Cs 3d, Pb 4f, and Br 3d spectra for the resulting quantum dots. The main peaks of Cs 3d, Pb 5f, and Br 4d in the quantum dots' spectra have binding energy positions similar to those of the bulk materials.[33] The Cs:Pb:Br ratio of the $CsPbBr_3$ quantum dots was calculated close to be 1:1:3, which was obtained from the ratios of XPS peak areas of survey spectra corrected by sensitivity factors from literature.[33]

The optical properties as-synthesized $CsPbBr_3$ quantum dots could be manipulated by anion exchange reactions using ZnI_2

DOI: 10.1021/acsnano.5b08193
ACS Nano 2016, 10, 3648−3657

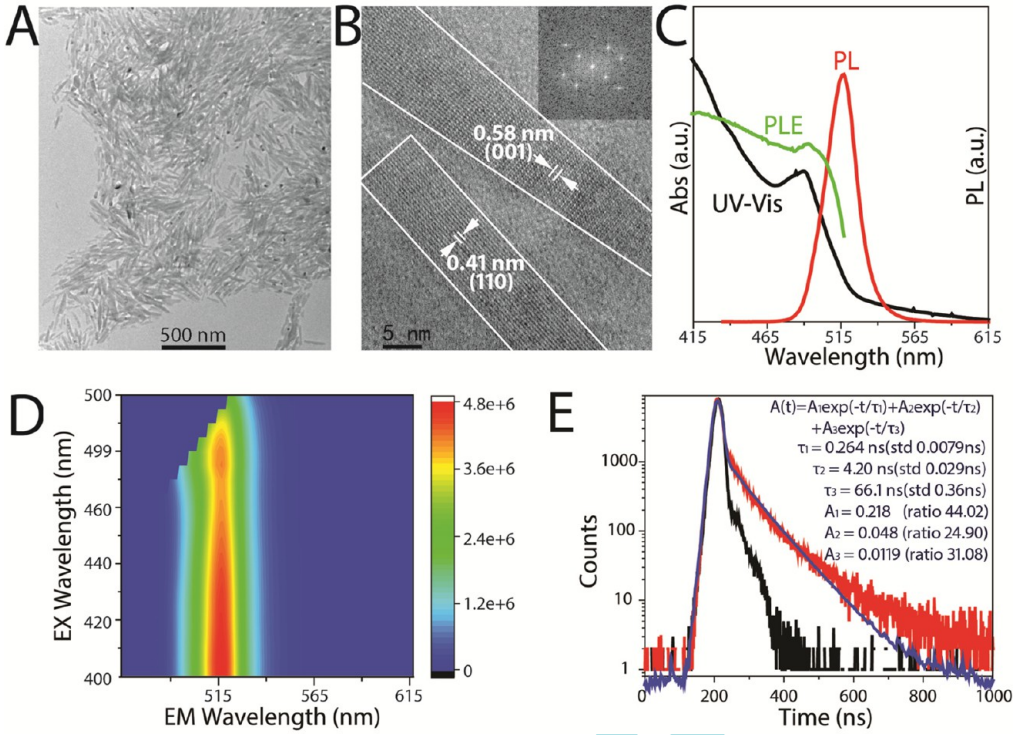

Figure 5. $CsPbBr_3$ nanorods synthesized using acetate acid and dodecylamine as ligands at room temperature. (A) Low- and (B) high-resolution TEM images of $CsPbBr_3$ nanorods. Inset in (B) is the corresponding FFTs of the image. (C) Optical absorption (black line), PL excitation (green line), and PL emission (red line) spectra of the $CsPbBr_3$ nanorods. (D) Graphical depictions of the pseudo colored PL intensity measured as a function of excitation wavelength. (E) Time-resolved PL decay and fitting curves of the light emission at 515 nm from $CsPbBr_3$ nanoplatelets with a 375 nm pulse laser.

or $ZnCl_2$ as the resources for I^- or Cl^-. The anion exchange reactions discussed here led either to a red shift (for the Br^- to I^-) or to a blue shift (for the Br^- to Cl^-) of the optical features (Figure 3E–G), corroborating the incorporation of the new anions. The exchange with the highly soluble zinc halides (ZnX_2) salts was generally done within a few minutes under stirring to record a full shift in the PL emission spectra. Furthermore, exchange was often complete with narrow and intense PL emission spectra. This is consistent with the recently reported $CsPbBr_3$ nanocubes using difference I^- or Cl^- resources.[20,21]

By changing the ligands used in the synthesis, *i.e.*, replacing hexanoic acid with oleic acid; and substitute octylamine for dodecylamine, while keeping other process the same as the $CsPbBr_3$ spherical quantum dots, we obtained well-crystallized $CsPbBr_3$ nanocubes. Figure 4A shows the typical TEM image of $CsPbBr_3$ nanocubes. It is observed that $CsPbBr_3$ nanocubes have edge lengths of ~9 nm with a size deviation of ±1 nm. From the HRTEM images (Figures 4B and S6), interplanar distances of 5.8 and 4.1 Å, corresponding to (001) and (110) crystal faces, could be easily identified. This indicates that the $CsPbX_3$ nanocrystals bound mainly {100} for nanocubes. Figure 4C shows an XRD pattern of the product, where the peaks at 2θ = 15.1, 21.5, 30.4, 34.2, and 37.6° correspond to diffractions from {001}, {110}, {002}, {210}, and {211} planes of orthorhombic $CsPbBr_3$, which confirmed the formation of $CsPbBr_3$ nanocubes with space group *Pbnm*(62); this is consistent with JCPDF #01-072-7929. As shown in Figure 4D, the first absorption onset of the colloidal solution of $CsPbBr_3$ nanocubes is around 508 nm (2.44 eV), while the PL emission peak is about 514 nm (2.41 eV); this means the Stokes shift is 6 nm, *i.e.*, 30 meV. Figure 4E and Figure S7 show the graphical depictions of PL intensity measured as a function of excitation wavelength for the nanocubes sample with different concentrations. In this image, the PL intensity is represented by the color at a particular excitation and emission energy.[34,35] As shown in Figure 4F, the time-resolved PL decay curve of the $CsPbBr_3$ nanocubes can be described by triexponential fitting; giving a short-lived PL lifetime (τ_1) of 5.18 ns with a percentage of 57.89%, an intermediate PL lifetime (τ_2) of 18.7 ns with a percentage of 29.95%, and a long-lived PL lifetime (τ_3) of 129 ns with a percentage of 12.16%. The long lifetime might be due to less nonradiative energy transfer to the trap states of the high quality $CsPbBr_3$ nanocubes synthesized at room temperature.[32]

When replacing acetate acid with oleic acid and substitute octylamine for dodecylamine, while keeping other process the same as the $CsPbBr_3$ spherical quantum dots, we obtained $CsPbBr_3$ nanorods. Figures 5A, S8 and S9 show the typical TEM and HRTEM images of $CsPbBr_3$ nanorods. It is observed that $CsPbBr_3$ nanorods have typical length of ~200 nm and diameter of ~10 nm. From the HRTEM image (Figures 5B and S9), interplanar distances of 5.8 and 4.1 Å, corresponding to (001) and (110) crystal faces, can be easily identified. This indicates the growth direction of $CsPbX_3$ nanorods along {100} directions. As shown in Figure 5C, the first absorption onset of the colloidal solution of $CsPbBr_3$ nanorods is around 465 nm (2.67 eV), while the PL emission peak is about 515 nm (2.41 eV). Figure 5D shows the graphical depictions of PL intensity measured as a function of excitation wavelength for the nanorods sample. As shown in Figure 5E, the time-resolved PL decay curve was fitted to triexponential decay functions: a

DOI: 10.1021/acsnano.5b08193
ACS Nano 2016, 10, 3648–3657

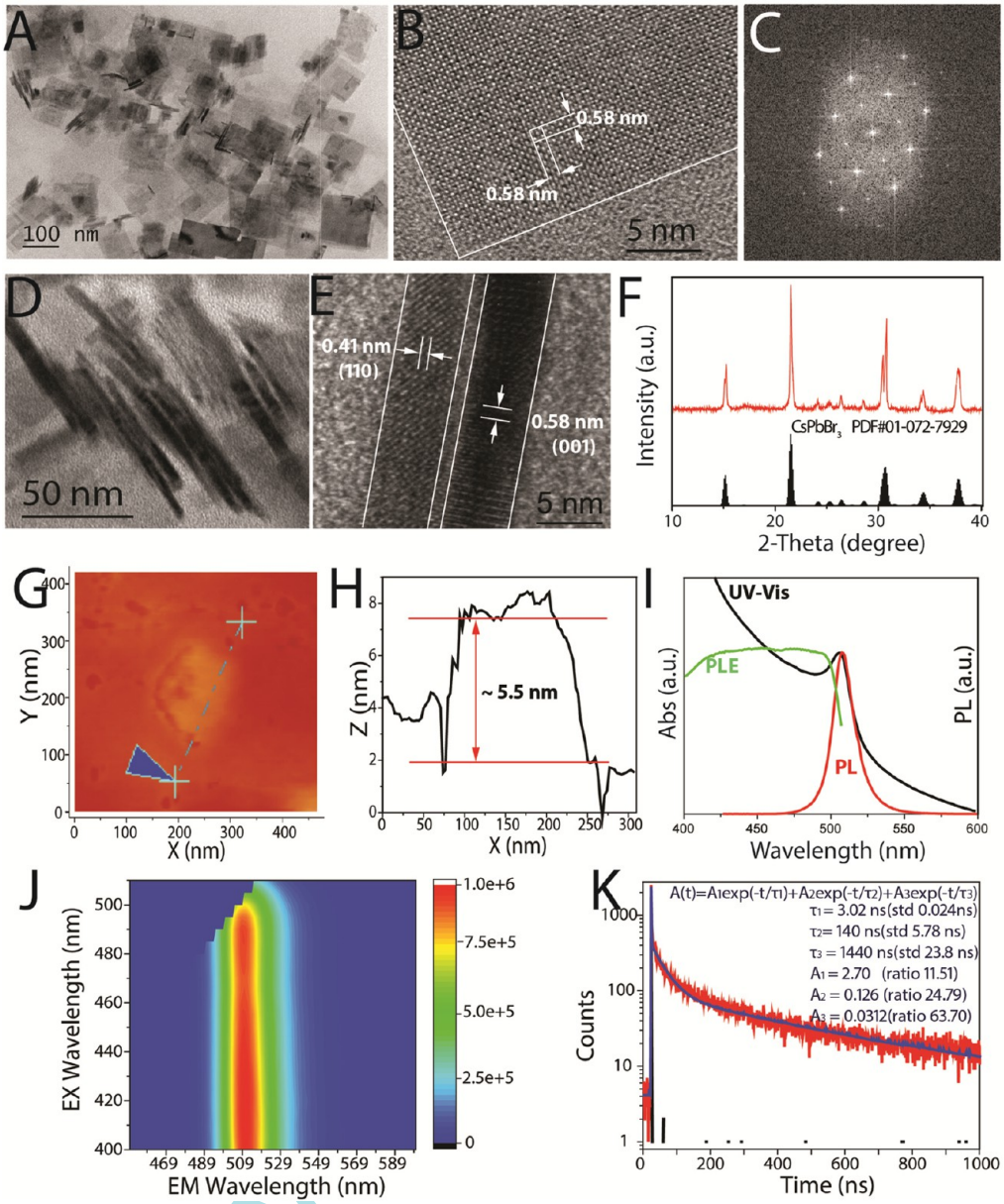

Figure 6. Few-unit-cell-thick $CsPbBr_3$ nanoplatelets synthesized using oleic acid and octylamine as ligands at room temperature. (A) Low-resolution TEM image of $CsPbBr_3$ nanoplatelets. (B and C) High-resolution TEM image and its corresponding FFTs of the corner of one typical flat lying $CsPbBr_3$ nanoplatelet. (D and E) Low- and (B) high-resolution TEM of the stacked nanoplatelets. (F) XRD pattern of $CsPbBr_3$ nanoplatelets. The white lines in B and D marked out the boundary of the atomic lattice structure of the nanoplatelets. (G and H) AFM topography micrograph depicting the $CdPbBr_3$ nanoplatelets with thickness around 5.5 nm, while the lateral dimension around 100 nm. (I) Optical absorption (black line), PL excitation (green line) and PL emission (red line) spectra of $CsPbBr_3$ nanoplatelets. (J) Graphical depictions of the pseudo colored PL intensity measured as a function of excitation wavelength. (K) Time-resolved PL decay and fitting curves of the light emission at 510 nm from $CsPbBr_3$ nanoplatelets with a 375 nm pulse laser.

short-lived PL lifetime (τ_1) of 0.264 ns with a percentage of 44.02% and an intermediate-lived PL lifetime (τ_2) of 4.20 ns with a percentage of 24.90%, and a long-lived PL lifetime (τ_3) of 66.1 ns with a percentage of 31.08%. To the best of our knowledge, this is the first report for colloidal synthesis and characterization of the $CsPbX_3$ nanorods in solution.

The growth of the single-crystal nanocrystals could be further manipulated to produce highly crystalline few-unit-cell-thick $CsPbBr_3$ nanoplatelets with well-defined square shape and large size by changing the type of the capping ligands, *i.e.*, hexanoic acid to oleic acid, while keeping other procedures the same as $CsPbBr_3$ quantum dots. Figures 6A–E and S10–S12 show the TEM and HRTEM images of $CsPbBr_3$ nanoplatelets. The $CsPbBr_3$ nanoplatelets have a typical edge length of ~100 nm. The high-resolution TEM image (Figure 6B) and its corresponding FFTs (Figure 6C) indicated the high crystallinity of the nanoplatelets sample. Similar images have also shown in Figure S10B,C. From the atomic lattice structure in the corner of one typical flat lying $CsPbBr_3$ nanoplatelet, we could identify the interplanar distances of 4.1 Å, corresponding to (110) crystal face. Figure 6D,E shows the low- and high-resolution TEM of the stacked nanoplatelets. The typical thickness of the nanoplatelets is about 5.2 nm with a size deviation of ±1.3 nm, corresponding to 4 monolayer $CsPbBr_3$.

DOI: 10.1021/acsnano.5b08193
ACS Nano 2016, 10, 3648–3657

It is observed that $CsPbBr_3$ nanoplatelets have side-view interplanar distances of 5.8 Å, corresponding to the (001) crystal faces, which can be easily identified. These results suggest that the few-unit-cell-thick $CsPbX_3$ nanoplatelets bound mainly {001} for the in-plane facets and {110} for the side-plane facets. Figure 6F shows their XRD pattern, where the peaks at 2θ = 15.1, 21.5, 30.4, 34.2, and 37.6° corresponding to diffractions {001}, {110}, {002}, {210}, and {211} planes of orthorhombic $CsPbBr_3$, which is also consistent with JCPDF #01-072-7929. The nanoplatelets sample was further characterized by atomic force microscopy (AFM) as shown in Figure 6G,H. Typically, large nanoplatelets of perovskite $CsPbBr_3$ of square/rectangular shapes with lateral dimensions of ~100 nm were readily measured. AFM image also shows the typical nanoplatelets thicknesses to be ~5.5 nm, which is in good agreement with the thickness of primary nanoplatelets (~5.2 nm) capped with organic ligands.

The UV−vis absorption, PL emission and excitation spectra of $CsPbBr_3$ nanoplatelets reveal the first absorption onset of around 508 nm and the PL emission peak of about 510 nm as shown in Figure 6I. The graphical depictions of PL intensity were measured as a function of excitation wavelength for the nanocubes sample (Figure 6J). Analysis of the entire time-resolved PL decay trace required three processes: a short-lifetime process (τ_1) of 3.02 ns with a percentage of 11.51%, an intermediate-lifetime process (τ_2) of 140 ns with a percentage of 24.79%, and a long-lived component (τ_3) of 1440 ns with a percentage of 63.70% as shown in Figure 6K. The increased lifetime could be attributed to the increased in-plane single-crystalline geometry of the nanoplatelets, and their PL decay mainly took place through exciton radiative recombination in the large crystal. Because of their atomically flat in-plane surface, the colloidal nanoplatelets typically have much less defects and surface states than nanocrystals with other shapes; this suggested that the short and intermediate-lifetime may originate from trap and or surface-state emissions.[32]

The formation of the variable shapes of $CsPbX_3$ nanocrystals with different organic acid and amine ligands was speculated by classic micellar transition mechanism, which depends on the electrostatic and hydrophobic interaction with the ions, the ligands, and the good and bad solvents.[36,37] Taking $CsPbBr_3$ spherical quantum dots as an example, polar hexanoic acid and octylamine surfactant self-assembly in nonpolar toluene solutions is a cooperative phenomenon and entropy driven process mainly governed by hydrophobic interaction. The size and shape of micelles depend on hydrocarbon tail, polar headgroup, and counterion in the ligand based formulation. We hypothesize that spherelike micelles formed at the concentration above the critical micelle concentration (CMC) and may grow to cuboid-like, rodlike, or even panel-like vesicles under different solvent conditions with the presence of ligands and ions. Thus, the formation of the different shaped nanocrystals might be achieved.

The Fourier transform infrared (FTIR) spectrum (Figure S13) of the spherical quantum dots sample shows mainly C−H stretches and bends, while the nanocube sample shows the typical C−O stretches and C−O bends, indicating the organic acid as the capping ligand. Both the nanorod and nanoplatelet samples were found to be capped with organic amine, while the former showed more N−H stretches and bends. These results indicate the selective adsorption of organic acid and amine ligands on the nanocrystal facets. From the XPS results of the spherical quantum dots (Figure S5), the N 1s peak is very small and could be negligible, indicating that *n*-octylamine might not act as a capping ligands for the formation of colloidal spherical $CsPbBr_3$ quantum dots, which is consistent with the above FTIR results, but different from the $NH_3CH_3PbBr_3$ quantum dots reported in the literature.[29] Further understanding of the exact relationships between the nanocrystals shapes and the ligand-mediated reprecipitation process is essential for achieving high quality perovskite $CsPbX_3$ nanocrystals at room temperature. Further studies will concentrate on these aspects.

CONCLUSIONS

A facile room-temperature, ligand-mediated approach has been developed for the shape-controlled synthesis of colloidal $CsPbX_3$ spherical quantum dots, nanocubes, nanorods, and few-unit-cell-thick nanoplatelets. We have demonstrated the dependence of the photoluminescence emission on the size, shape, and composition, which is readily manipulated over the visible spectral region from 380 to 693 nm. Furthermore, the shape-dependent photoluminescence decay lifetime of the $CsPbX_3$ nanocrystals has been determined to be several to tens to hundreds of nanoseconds. Further work to explore other optical properties and technological applications is currently underway. We envision that the shape-controlled $CsPbX_3$ perovskites nanocrystals will find widespread use in applications, such as lasing, light-emitting diodes, photovoltaics, solar concentrators, and photon detection. By the suitable choice of sources and/or synthetic parameters, it is reasonable to expect that the present methods can be extended to the synthesis of other perovskite nanocrystals like AMX_3 (A = Rb^+, Cs^+; M = Ge^{2+}, Sn^{2+}; X = F^-, Cl^-, Br^-, I^-, or combinations thereof) as well.

MATERIALS AND METHODS

Materials. Cs_2CO_3 (Aladdin, 99.9%), $PbBr_2$ (Aladdin, 99.0%), PbI_2 (Aladdin, 98.0%), ZnI_2 (Alfa Aesar, 98%), $ZnCl_2$ (Shanghai Xinbao Fine Chemical Co. Ltd., 98%), octadecene (ODE, Aladdin, 90%), *N*,*N*-dimethylformamide (DMF, Sinopharm Chemical Reagent Co. Ltd., AR), oleic acid ($CH_3(CH_2)_7CH{=}CH(CH_2)_7COOH$, 90%, Aladdin, AR), hexanoic acid ($CH_3CH_2CH_2CH_2CH_2COOH$, Aladdin, 99.0%), octylamine ($CH_3CH_2CH_2CH_2CH_2CH_2CH_2CH_2NH_2$, Aladdin, 99%), dodecylamine ($CH_3CH_2CH_2CH_2CH_2CH_2CH_2CH_2CH_2$-$CH_2CH_2CH_2NH_2$, Sinopharm Chemical Reagents Co. Ltd., CP), and toluene (Shanghai Lingfeng Chemical Reagent Co. Ltd., ≥ 99.5%) were purchased and used without further purification.

Preparation of Cs−Oleate. Cs_2CO_3 (0.814 g) was loaded into a 100 mL, 3-neck flask along with octadecene (10 mL, ODE) and oleic acid (2.5 mL), and the mixture was dried for 1 h at 120 °C and then heated under N_2 to 150 °C until all Cs_2CO_3 reacted with oleic acid. Since Cs−oleate precipitates out of ODE at room temperature, it has to be preheated to make it soluble before usage.

Synthesis of $CsPbBr_3$ Spherical Quantum Dots. In a typical synthesis of $CsPbBr_3$ spherical quantum dots, DMF (1 mL) and $PbBr_2$ (0.05 mmol) were loaded into a 5 mL flask. Then, hexanoic acid (0.1 mmol) and octylamine (0.1 mmol) were added. After complete solubilization of $PbBr_2$, Cs−oleate solution (0.05 mL, 0.4 mol/L in ODE, prepared as shown in the experimental section) was added. Finally, 0.05 mL of mixed solution was added into a new flask along with toluene (2 mL). For scale-up synthesis, *N*,*N*-dimethylformamide (500 mL, DMF) and $PbBr_2$ (25 mmol) were loaded into a 1 L flask. Hexanoic acid (50 mmol) and *n*-octylamine (50 mmol) were added. After complete solubilization of $PbBr_2$, Cs−oleate solution (25 mL, 0.4 M in ODE, prepared as described above) was added. Then, 12.5 mL of hybrid solution was added into a 1 L flask along with toluene (500 mL).

Synthesis of Other $CsPbX_3$ Spherical Quantum Dots. The synthesis of other $CsPbX_3$ nanocrystals was similar to that of $CsPbBr_3$,

DOI: 10.1021/acsnano.5b08193
ACS Nano 2016, 10, 3648−3657

except for the use of 0.05 mmol PbI_2, $PbCl_2$, or PbI_2 and $PbCl_2$ mixture with their corresponding molar ratio of 1:1, respectively, instead of 0.05 mmol $PbBr_2$. For example, in a typical synthesis of $CsPbI_3$ quantum dots, *N*,*N*-dimethylformamide (2 mL, DMF) and PbI_2 (0.1 mmol) were loaded into a 5 mL flask. Hexanoic acid (0.6 mmol) and *n*-octylamine (0.6 mmol) were added. After complete solubilization of PbI_2, Cs−oleate solution (0.1 mL, 0.4 M in ODE, prepared as described above) was added. Then, 0.005 mL of hybrid solution was added into a 5 mL flask along with toluene (2 mL). A certain amount (*e.g.*, 0.2 mmol) of ZnI_2 was added with PbI_2 (0.1 mmol) to increase the intensity of the PL emission.

Anion Exchange Reactions with $CsPbBr_3$ Spherical Quantum Dots. The anion exchange reactions were conducted in a 15 mL flask. A total of 0.02 mL of $CsPbBr_3$ spherical quantum dots synthesized in hexanoic acid and octylamine was dispersed in 4 mL of toluene and the mixture was used as the precursor. ZnI_2 (6 mg) used as the anion source was mixed with toluene (12 mL) in a 15 mL flask and fully dissolved before use. After complete dispersion in toluene, certain amount of ZnI_2 was injected into $CsPbBr_3$ parent quantum dots solution to initiate the anion-exchange. Br^- to Cl^- anion exchange reactions were conducted using a similar protocol. The evolution of the PL emission peak maxima as a result of anion exchange has been completed within tens of seconds to a few minutes. After reaction, the emission wavelength of obtained NCs was detected by fluorimeter.

Synthesis of $CsPbBr_3$ Nanocubes. *N*,*N*-Dimethylformamide (2 mL) and $PbBr_2$ (0.1 mmol) were loaded into a 5 mL flask. Oleic acid (1.55 mmol) and dodecylamine (0.086 mmol) were added. After complete solubilization of $PbBr_2$, Cs−oleate solution (0.1 mL, 0.4 M in ODE, prepared as described above) was added. Then, 0.05 mL of hybrid solution was added into a 5 mL flask along with toluene (2 mL).

Synthesis of $CsPbBr_3$ Nanorods. *N*,*N*-Dimethylformamide (2 mL) and $PbBr_2$ (0.1 mmol) were loaded into a 5 mL flask. Acetate acid (1.55 mmol) and dodecylamine (0.086 mmol) were added. After complete solubilization of $PbBr_2$, Cs−oleate solution (0.1 mL, 0.4 M in ODE, prepared as described above) was added. Then, 0.05 mL of hybrid solution was added into a 5 mL flask along with toluene (2 mL).

Synthesis of $CsPbBr_3$ Nanoplatelets. *N*,*N*-Dimethylformamide (2 mL) and $PbBr_2$ (0.1 mmol) were loaded into a 5 mL flask. Oleic acid (0.031 mmol) and octylamine (0.362 mmol) were added. After complete solubilization of $PbBr_2$, Cs−oleate solution (0.1 mL, 0.4 M in ODE, prepared as described above) was added. Then, 0.05 mL of hybrid solution was added into a 5 mL flask along with toluene (2 mL).

Characterizations. X-ray powder diffraction (XRD) measurements were employed a Bruker AXS D8 X-ray diffractometer equipped with monochromatized Cu Kα radiation (λ = 1.5418 Å). Fourier transform infrared (FTIR) spectra were recorded with a Varian 3100 FT−IR spectrometer at room temperature. X-ray photoelectron spectroscopy (XPS) measurements were performed using an achromatic Al Kα source (1486.6 eV) and a double pass cylindrical mirror analyzer (ULVAC-PHI 5000 VersaProbe). The atomic ratios were obtained from ratios of XPS peak areas of the high-resolution spectra corrected by sensitivity factors from the literature. Transmission electron microscopy (TEM) and high-resolution TEM were performed on a FEI Tecnai G2 F20 electron microscope operating at 200 kV. Ultraviolet and visible absorption (UV−vis) spectra were recorded with a Beituo DUV-18S2 and a Shimadzu UV-3600 plus spectrophotometer at room temperature. The topography of the nanoplatelets was investigated using a Nanoscope Dimension CSPM5500 Atomic Force Microscope working in tapping mode. The EDS spectra were investigated using field-emission scanning electron microscopy (FESEM; Hitachi S-4800) with an energy-dispersive X-ray (EDS) analyzer. PL excitation and emission spectra were measured with a Hitachi F4500 fluorescence spectrophotometer, a home-made fiber fluorimeter system, a compact spectrometer purchased from Thorlabs, or a Horiba PTI QuantaMaster 400 steady-state fluorescence system at room temperature. The fluorescence decay processes were recorded with time-correlated single-photon counting (TCSPC) technique on an Edinburgh FLS920 phosphorescence lifetime system equipped with a 375 nm, 45 ps pulse width laser and a time-correlated single-photon counting system at room temperature. The standard silica particles samples dispersed in water were used as the standard to eliminate the effect of the scattering from the samples. Time-resolved PL decay curves were fitted[31] to a triexponential (see eqs 1 and 2) decay curves of

$$A(t) = A_1 \exp\left(-\frac{t}{\tau_1}\right) + A_2 \exp\left(-\frac{t}{\tau_2}\right) + A_3 \exp\left(-\frac{t}{\tau_3}\right) \quad (1)$$

The average lifetimes were calculated using

$$\tau_{avg} = (A_1\tau_1^2 + A_2\tau_2^2 + A_3\tau_3^2)/(A_1\tau_1 + A_2\tau_2 + A_3\tau_3) \quad (2)$$

ASSOCIATED CONTENT

Supporting Information

The Supporting Information is available free of charge on the ACS Publications website at DOI: 10.1021/acsnano.5b08193.

Additional experimental data, HRTRM, XPS, FTIR results, including Figures S1−S14 and Table S1 (PDF)

AUTHOR INFORMATION

Corresponding Author

*E-mail: dengz@nju.edu.cn.

Notes

The authors declare no competing financial interest.

ACKNOWLEDGMENTS

This work was supported by Thousand Talents Program for Young Researchers, National Natural Science Foundation of China (Grant No. 51502130), Natural Science Foundation of Jiangsu Province (Grant No. SBK2015043303), Shuangchuang Program of Jiangsu Province, Fundamental Research Funds for Central Universities, and Nanjing University. TEM and XPS experiments were carried out in part in Center of Modern Analysis at Nanjing University.

REFERENCES

(1) Gratzel, M. The Light and Shade of Perovskite Solar Cells. *Nat. Mater.* **2014**, *13*, 838−842.

(2) Stoumpos, C. C.; Kanatzidis, M. G. The Renaissance of Halide Perovskites and Their Evolution as Emerging Semiconductors. *Acc. Chem. Res.* **2015**, *48*, 2791−2802.

(3) Boix, P. P.; Agarwala, S.; Koh, T. M.; Mathews, N.; Mhaisalkar, S. G. Perovskite Solar Cells Beyond Methylammonium Lead Iodide. *J. Phys. Chem. Lett.* **2015**, *6*, 898−907.

(4) Fu, Y.; Meng, F.; Rowley, M. B.; Thompson, B. J.; Shearer, M. J.; Ma, D.; Hamers, R. J.; Wright, J. C.; Jin, S. Solution Growth of Single Crystal Methylammonium Lead Halide Perovskite Nanostructures for Optoelectronic and Photovoltaic Applications. *J. Am. Chem. Soc.* **2015**, *137*, 5810−5818.

(5) Green, M. A.; Ho-Baillie, A.; Snaith, H. J. The Emergence of Perovskite Solar Cells. *Nat. Photonics* **2014**, *8*, 506−514.

(6) Zhou, H. P.; Chen, Q.; Li, G.; Luo, S.; Song, T. B.; Duan, H. S.; Hong, Z. R.; You, J. B.; Liu, Y. S.; Yang, Y. Interface Engineering of Highly Efficient Perovskite Solar Cells. *Science* **2014**, *345*, 542−546.

(7) Schmidt, L. C.; Pertegás, A.; González-Carrero, S.; Malinkiewicz, O.; Agouram, S.; Mínguez Espallargas, G.; Bolink, H. J.; Galian, R. E.; Pérez-Prieto, J. Nontemplate Synthesis of $CH_3NH_3PbBr_3$ Perovskite Nanoparticles. *J. Am. Chem. Soc.* **2014**, *136*, 850−853.

(8) Tian, W.; Zhao, C.; Leng, J.; Cui, R.; Jin, S. Visualizing Carrier Diffusion in Individual Single−Crystal Organolead Halide Perovskite Nanowires and Nanoplates. *J. Am. Chem. Soc.* **2015**, *137*, 12458−12461.

DOI: 10.1021/acsnano.5b08193
ACS Nano 2016, 10, 3648−3657

(9) Sichert, J. A.; Tong, Y.; Mutz, N.; Vollmer, M.; Fischer, S.; Milowska, K. Z.; García Cortadella, R.; Nickel, B.; Cardenas-Daw, C.; Stolarczyk, J. K.; Urban, A. S.; Feldmann, J. Quantum Size Effect in Organometal Halide Perovskite Nanoplatelets. *Nano Lett.* **2015**, *15*, 6521−6527.
(10) Dou, L.; Wong, A. B.; Yu, Y.; Lai, M.; Kornienko, N.; Eaton, S. W.; Fu, A.; Bischak, C. G.; Ma, J.; Ding, T.; Ginsberg, N. S.; Wang, L.−W.; Alivisatos, A. P.; Yang, P. Atomically Thin Two−Dimensional Organic−Inorganic Hybrid Perovskites. *Science* **2015**, *349*, 1518−1521.
(11) Zhang, D.; Eaton, S. W.; Yu, Y.; Dou, L.; Yang, P. Solution−Phase Synthesis of Cesium Lead Halide Perovskite Nanowires. *J. Am. Chem. Soc.* **2015**, *137*, 9230−9233.
(12) Yakunin, S.; Protesescu, L.; Krieg, F.; Bodnarchuk, M. I.; Nedelcu, G.; Humer, M.; De Luca, G.; Fiebig, M.; Heiss, W.; Kovalenko, M. V. Low−Threshold Amplified Spontaneous Emission and Lasing from Colloidal Nanocrystals of Caesium Lead Halide Perovskites. *Nat. Commun.* **2015**, *6*, 8056.
(13) Song, J.; Li, J.; Li, X.; Xu, L.; Dong, Y.; Zeng, H. Quantum Dot Light−Emitting Diodes Based on Inorganic Perovskite Cesium Lead Halides ($CsPbX_3$). *Adv. Mater.* **2015**, *27*, 7162−7167.
(14) Wells, H. L. Über die Cäsium− und Kalium−Bleihalogenide. *Z. Anorg. Chem.* **1893**, *3*, 195−210.
(15) Moller, C. K. Crystal Structure and Photoconductivity of Caesium Plumbohalides. *Nature* **1958**, *182*, 1436−1436.
(16) Moller, C. K. A Phase Transition in Caesium Plumbochloride. *Nature* **1957**, *180*, 981−982.
(17) Protesescu, L.; Yakunin, S.; Bodnarchuk, M. I.; Krieg, F.; Caputo, R.; Hendon, C. H.; Yang, R. X.; Walsh, A.; Kovalenko, M. V. Nanocrystals of Cesium Lead Halide Perovskites ($CsPbX_3$ X = Cl, Br, and I) Novel Optoelectronic Materials Showing Bright Emission with Wide Color Gamut. *Nano Lett.* **2015**, *15*, 3692−3696.
(18) Bekenstein, Y.; Koscher, B. A.; Eaton, S. W.; Yang, P.; Alivisatos, A. P. Highly Luminescent Colloidal Nanoplates of Perovskite Cesium Lead Halide and Their Oriented Assemblies. *J. Am. Chem. Soc.* **2015**, *137*, 16008−16011.
(19) Stoumpos, C. C.; Malliakas, C. D.; Peters, J. A.; Liu, Z. F.; Sebastian, M.; Im, J.; Chasapis, T. C.; Wibowo, A. C.; Chung, D. Y.; Freeman, A. J.; et al. Crystal Growth of the Perovskite Semiconductor $CsPbBr_3$ A New Material for High−Energy Radiation Detection. *Cryst. Growth Des.* **2013**, *13*, 2722−2727.
(20) Akkerman, Q. A.; D'Innocenzo, V.; Accornero, S.; Scarpellini, A.; Petrozza, A.; Prato, M.; Manna, L. Tuning the Optical Properties of Cesium Lead Halide Perovskite Nanocrystals by Anion Exchange Reactions. *J. Am. Chem. Soc.* **2015**, *137*, 10276−10281.
(21) Nedelcu, G.; Protesescu, L.; Yakunin, S.; Bodnarchuk, M. I.; Grotevent, M. J.; Kovalenko, M. V. Fast Anion−Exchange in Highly Luminescent Nanocrystals of Cesium Lead Halide Perovskites ($CsPbX_3$, X = Cl, Br, I). *Nano Lett.* **2015**, *15*, 5635−5640.
(22) Park, Y. S.; Guo, S.; Makarov, N. S.; Klimov, V. I. Room Temperature Single−Photon Emission from Individual Perovskite Quantum Dots. *ACS Nano* **2015**, *9*, 10386−10393.
(23) Wu, K.; Liang, G.; Shang, Q.; Ren, Y.; Kong, D.; Lian, T. Ultrafast Interfacial Electron and Hole Transfer from $CsPbBr_3$ Perovskite Quantum Dots. *J. Am. Chem. Soc.* **2015**, *137*, 12792−12795.
(24) Kovalenko, M. V.; Manna, L.; Cabot, A.; Hens, Z.; Talapin, D. V.; Kagan, C. R.; Klimov, V. I.; Rogach, A. L.; Reiss, P.; Milliron, D. J.; Guyot-Sionnnest, P.; Konstantatos, G.; Parak, W. J.; Hyeon, T.; Korgel, B. A.; Murray, C. B.; Heiss, W. Prospects of Nanoscience with Nanocrystals. *ACS Nano* **2015**, *9*, 1012−1057.
(25) Grim, J. Q.; Manna, L.; Moreels, I. A Sustainable Future for Photonic Colloidal Nanocrystals. *Chem. Soc. Rev.* **2015**, *44*, 5897−5914.
(26) Zhu, F.; Men, L.; Guo, Y.; Zhu, Q.; Bhattacharjee, U.; Goodwin, P. M.; Petrich, J. W.; Smith, E. A.; Vela, J. Shape Evolution and Single Particle Luminescence of Organometal Halide Perovskite Nanocrystals. *ACS Nano* **2015**, *9*, 2948−2959.
(27) Huang, H.; Zhao, F.; Liu, L.; Zhang, F.; Wu, X.−g.; Shi, L.; Zou, B.; Pei, Q.; Zhong, H. Emulsion Synthesis of Size−Tunable $CH_3NH_3PbBr_3$ Quantum Dots An Alternative Route toward Efficient Light−Emitting Diodes. *ACS Appl. Mater. Interfaces* **2015**, *7*, 28128−28133.
(28) Akkerman, Q. A.; Motti, S. G.; Srimath Kandada, A. R.; Mosconi, E.; D'Innocenzo, V.; Bertoni, G.; Marras, S.; Kamino, B. A.; Miranda, L.; De Angelis, F.; Petrozza, A.; Prato, M.; Manna, L. Solution Synthesis Approach to Colloidal Cesium Lead Halide Perovskite Nanoplatelets with Monolayer−Level Thickness Control. *J. Am. Chem. Soc.* **2016**, *138*, 1010−1016.
(29) Zhang, F.; Zhong, H.; Chen, C.; Wu, X. G.; Hu, X.; Huang, H.; Han, J.; Zou, B.; Dong, Y. Brightly Luminescent and Color−Tunable Colloidal $CH_3NH_3PbX_3$ (X = Br, I, Cl) Quantum Dots Potential Alternatives for Display Technology. *ACS Nano* **2015**, *9*, 4533−4542.
(30) Huang, H.; Susha, A. S.; Kershaw, S. V.; Hung, T. F.; Rogach, A. L. Control of Emission Color of High Quantum Yield $CH_3NH_3PbBr_3$ Perovskite Quantum Dots by Precipitation Temperature. *Adv. Sci.* **2015**, *2*, 1500194.
(31) Deng, Z.; Schulz, O.; Lin, S.; Ding, B.; Liu, X.; Wei, X.; Ros, R.; Yan, H.; Liu, Y. Aqueous Synthesis of Zinc Blende CdTe/CdS Magic−Core/Thick−Shell Tetrahedral−Shaped Nanocrystals with Emission Tunable to Near−Infrared. *J. Am. Chem. Soc.* **2010**, *132*, 5592−5593.
(32) Yantara, N.; Bhaumik, S.; Yan, F.; Sabba, D.; Dewi, H. A.; Mathews, N.; Boix, P. P.; Demir, H. V.; Mhaisalkar, S. Inorganic Halide Perovskites for Efficient Light−Emitting Diodes. *J. Phys. Chem. Lett.* **2015**, *6*, 4360−4364.
(33) Moulder, J.; Stickie, W.; Sobal, P.; Bomber, K. *Handbook of X-ray Photoelectron Spectroscopy*; Perkin-Elmer Corp., 1992.
(34) Bachilo, S. M.; Strano, M. S.; Kittrell, C.; Hauge, R. H.; Smalley, R. E.; Weisman, R. B. Structure−Assigned Optical Spectra of Single−Walled Carbon Nanotubes. *Science* **2002**, *298*, 2361−2366.
(35) Zhong, H.; Nagy, M.; Jones, M.; Scholes, G. D. Electronic States and Exciton Fine Structure in Colloidal CdTe Nanocrystals. *J. Phys. Chem. C* **2009**, *113*, 10465−10470.
(36) Tanford, C. Theory of Micelle Formation in Aqueous Solutions. *J. Phys. Chem.* **1974**, *78*, 2469−2479.
(37) Eastoe, J.; Hollamby, M. J.; Hudson, L. Recent Advances in Nanoparticle Synthesis with Reversed Micelles. *Adv. Colloid Interface Sci.* **2006**, *128−130*, 5−15.

DOI: 10.1021/acsnano.5b08193
ACS Nano 2016, 10, 3648−3657